^{87}Rb D_1 isoclinic point

N. P. Wells and J. C. Camparo
Physical Sciences Laboratories, The Aerospace Corporation, P. O. Box 92957, Los Angeles, California 90009, USA
(Received 20 September 2010; published 7 December 2010)

In the research presented here, we reconsider the problem of obtaining stable resonant features in linear absorption spectroscopy, which has application to ultraminiature atomic physics where sub-Doppler spectroscopic techniques are not always optimal. In particular, we consider the applicability of isoclinic points for precision atomic spectroscopy. These are defined as "[a] wavelength, wave number, or frequency at which the first derivative of an absorption spectrum of a sample does not change upon a chemical reaction or physical change of the sample," and we demonstrate the existence of isoclinic points in the D_1 spectra of $I = 3/2$ alkali-metal isotopes, where I is the nuclear spin. We then consider the D_1 isoclinic point of ^{87}Rb in detail, showing that a slight ^{85}Rb contamination in real ^{87}Rb samples should have no significant effect on the frequency stability of the isoclinic point and that optical pumping by a linearly polarized laser should also not affect the isoclinic point's stability (i.e., the isoclinic point is insensitive to laser intensity). Finally, we perform an experiment demonstrating that the ^{87}Rb D_1 isoclinic point has a temperature shift more than an order of magnitude smaller than that of the most isolated transition in the ^{87}Rb D_1 spectrum.

DOI: 10.1103/PhysRevA.82.062505 PACS number(s): 32.70.Cs, 32.30.Jc, 06.30.Ft

I. INTRODUCTION

Ultraminiature atomic physics (UAP) is essentially precision spectroscopy aimed at generating and accurately probing an atomic interaction over millimeter or smaller scales, while at the same time severely constraining overall size and power. Today, UAP is most readily identified with the chip-scale atomic clock [1,2] and the chip-scale atomic magnetometer [3], each of which is receiving considerable attention due to their basic and applied physics applications. Though it might be natural to assume that the underlying atomic physics of UAP is well understood, and that miniaturization only involves the solution of engineering (albeit nontrivial) problems, the reality differs substantially. The constraints of UAP force the atomic phenomena to take place under physical conditions that are often not encountered or specifically avoided in routine laboratory study, and these conditions can bring new and sometimes significant dimensions to the atomic physics. For example, in UAP alkali-metal atom number densities are large in order to achieve significant photon absorption over ultraminiature path lengths. Consequently, rapid alkali-metal/alkali-metal spin exchange [4] can often play an important role in UAP, and at present the basic phenomenon of rapid spin exchange has not been fully explored [5,6]. At issue in the present work is the influence of vapor temperature on the resonant features of Doppler-broadened optical absorption spectra, and in particular their frequency stability. Though this would seem a well-worn question of atomic physics, with answers decades old, the constraints of UAP have forced its re-examination.

Routinely in UAP diode lasers are employed for spectroscopy and/or optical pumping [7], with the laser locked to an atomic absorption line in order to ensure its long-term wavelength stability [8,9]. Laser stability is critical, not only because variations in wavelength yield variations in the spectroscopic signals of interest but also because variations in laser wavelength can alter the atoms' energy level structure through the light-shift effect (i.e., the ac Stark shift) [10,11]. Obviously, sub-Doppler spectroscopy [12] is the foremost means of achieving laser wavelength stability, and it is routinely employed in many laboratories for that purpose [13]. However, for UAP linear absorption spectroscopy (LAS) has overriding advantages. In particular, linear spectroscopy allows for simplicity (and thereby compactness) of design, and without the need of overlapped, counterpropagating beams there is much less sensitivity to microphonics. Unfortunately, the Doppler-broadened optical absorption lines of LAS typically overlap, and as a consequence the peaks of the absorption lines shift slightly (but non-negligibly) with the vapor's temperature.

In the present work, we consider the role of isoclinic points in precision linear optical spectroscopy. According to the IUPAC Goldbook, an isoclinic point is defined as "[a] wavelength, wave number, or frequency at which the first derivative of an absorption spectrum of a sample does not change upon a chemical reaction or physical change of the sample" [14], and to date these have been principally employed by biochemists in electron-spin resonance spectroscopy [15]. Biochemists exploit isoclinic points as markers that strongly suggest "the presence of a linear combination of two interconverting species that are spectrally distinguishable" [16]. Here, we demonstrate that optical analogs of ESR isoclinic points exist for alkali-metal atoms with nuclear spin I equal to $3/2$ and that the frequencies of these isoclinic points are effectively independent of vapor temperature. Moreover, for linearly polarized light these isoclinic points are unaffected by optical pumping, implying that their frequencies are also insensitive to laser intensity.

II. ISOCLINIC POINTS FOR PRECISION SPECTROSCOPY

Doppler broadening is routinely problematic in linear, vapor-phase, absorption spectroscopy, especially when it leads to overlapped optical transitions. The issue is not always the loss of resolution (which can often be mitigated, to a degree, through improvements in the signal-to-noise ratio) but the fact that overlapping transitions have peak absorption frequencies that shift with vapor temperature. For example, as illustrated in Fig. 1 for the D_1 transition of ^{87}Rb, the Doppler-broadened

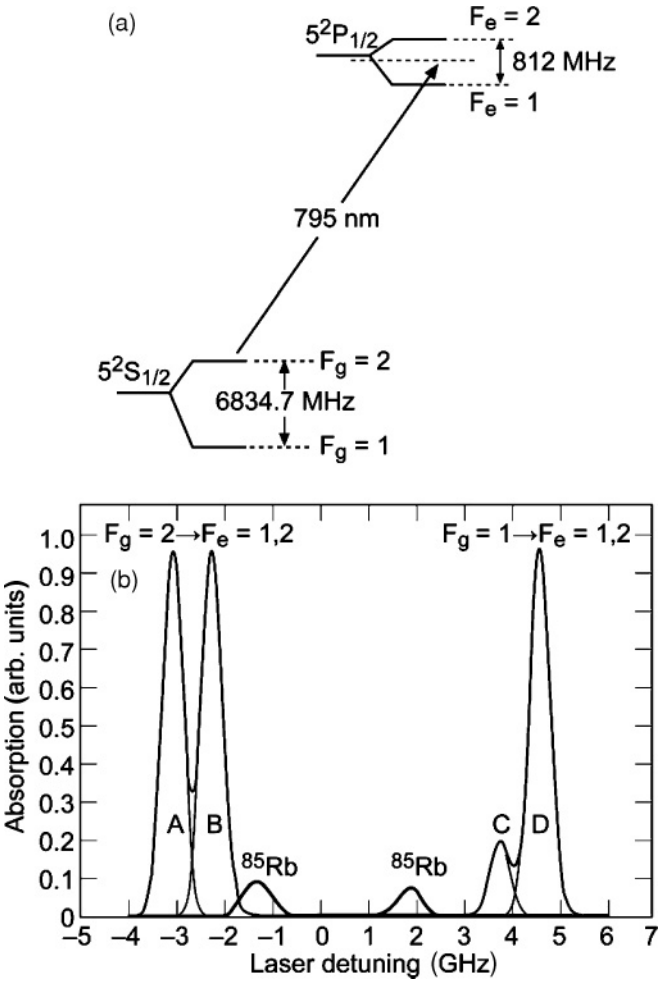

FIG. 1. (a) Energy level diagram for the ^{87}Rb D_1 transition at 795 nm. (b) Theoretical absorption spectrum of the Rb D_1 transition near room temperature. For illustrative purposes, we have assumed a ^{85}Rb fractional abundance of 10%; for naturally occurring Rb the isotope abundances are 72% ^{85}Rb and 28% ^{87}Rb.

absorption lines corresponding to transitions from the $5^2S_{1/2}$ ground-state hyperfine levels to the $5^2P_{1/2}$ excited-state hyperfine levels overlap. Consequently, the peaks of the absorption lines are "pulled" relative to the transitions' true resonant frequencies by the wings of the neighboring lines. Change the degree of spectral overlap, and the absorption lines' peak frequencies will shift. Since the Doppler-broadened widths of absorption lines change with temperature, so too does the degree of spectral overlap among the transitions; this in turn gives the peak frequencies of a linear vapor-phase absorption spectrum a sensitivity to vapor temperature.

To illustrate the problem more quantitatively, consider two neighboring Doppler-broadened transitions, A and B, as illustrated in Fig. 1, where w_D is the Doppler-broadened full width at half maximum (FWHM). For a laser frequency ω_L tuned near these absorption lines, the irradiance transmitted by a vapor of length L will be given by

$$I(L) = I_o \exp\{-NL[\sigma_A(\Delta_A) + \sigma_B(\Delta_B)]\}, \tag{1}$$

Here, $\sigma_J(\Delta_J)$ is the cross section of the Jth resonance and Δ_J is the detuning from the true resonant frequency of the transition: $\Delta_J = \omega_L - \omega_J$. Taking the derivative of Eq. (1) with respect to laser frequency we have

$$\frac{dI(L)}{d\omega_L} = -NLe^{-NL[\sigma_A(\Delta_A)+\sigma_B(\Delta_B)]}\left(\frac{d\sigma_A}{d\omega_L} + \frac{d\sigma_B}{d\omega_L}\right), \tag{2a}$$

which provides a necessary condition for local extrema in the atoms' absorption spectrum:

$$\left(\frac{d\sigma_A}{d\omega_L} + \frac{d\sigma_B}{d\omega_L}\right) = 0. \tag{2b}$$

For the case of the maximum located near absorption line A in Fig. 1, this procedure yields a peak frequency for the A transition (i.e., $\Delta_A \ll \Delta_B$) given by

$$\omega_{pA} = \omega_A - \Delta_B \left(\frac{\sigma_{pB}}{\sigma_{pA}}\right) e^{-4\ln(2)(\Delta_B/w_D)^2} \tag{3a}$$

or

$$\omega_{pA} \cong \omega_A - (\omega_A - \omega_B)\left(\frac{\sigma_{pB}}{\sigma_{pA}}\right) e^{-4\ln(2)[(\omega_A-\omega_B)/w_D]^2}, \tag{3b}$$

where σ_{pJ} is the peak absorption cross section of the Jth transition and where ω_{pA} is seen to have a temperature-dependent shift due to the temperature sensitivity of the Doppler width. (To be clear, ω_{pA} is the peak frequency of the absorption line, while ω_A is the transition's intrinsic resonant frequency: $(E_e - E_g)/\hbar$.) In particular, for small changes about some reference temperature T_o, and defining Δ_{AB} as $\omega_A - \omega_B$, the peak frequency of the transition will vary like

$$\frac{\delta\omega_{pA}}{\delta T} \cong -4\ln(2)\frac{\Delta_{AB}}{T_o}\left[\frac{\sigma_B(\Delta_{AB})}{\sigma_{pA}}\right]\left[\frac{\Delta_{AB}}{w_D(T_o)}\right]^2. \tag{4}$$

For absorption line A in Fig. 1 at 35°C, this yields $\delta\omega_{aP}/\delta T \cong 16$ kHz/°C, or in fractional frequency, y, 4.2×10^{-11}/°C (i.e., $y \equiv \delta\omega/\omega_o$). This is a relatively large temperature sensitivity for the peak frequency of a transition and demonstrates the significant role that a vapor's temperature variations can play in precision spectroscopy.

In obtaining Eq. (4), it is clear that on-resonance the two overlapped transitions do not contribute equally to the total cross section, and it is this asymmetry that causes the spectral feature's temperature shift. Conversely, near the midpoint between two overlapped resonances, both cross sections make significant contributions to the total cross section. In particular, if we define ω_m as the frequency corresponding to a local minimum near the midpoint between two overlapped transitions, then for reasonably resolved, Doppler-broadened absorption lines (and assuming $\sigma_{pA} \cong \sigma_{pB}$) it is straightforward to show that

$$\omega_m \cong \left(\frac{\omega_A + \omega_B}{2}\right) - \frac{(\sigma_{pA} - \sigma_{pB})}{(\sigma_{pA} + \sigma_{pB})}\frac{\Delta_{AB} w_D^2}{4\ln(2)\Delta_{AB}^2 - 2w_D^2}. \tag{5}$$

[In deriving Eq. (5), we have taken $\omega = (\omega_A + \omega_B)/2 + \delta$, and ignored terms of order $(\delta/w_D)^2$ and higher.] In this case, a temperature shift of the minimum only arises when the absorption cross sections of the two transitions are unequal. When σ_{pA} equals σ_{pB} the second term on the right-hand side of Eq. (5) is identically zero, and the frequency of the local minimum equals the intrinsic midpoint frequency of the two transitions independent of temperature: the midpoint frequency is an isoclinic point.

Notwithstanding the above discussion, for precision spectroscopy it is important to note that isoclinic points are idealizations: no vapor-phase atomic or molecular spectral feature will ever be insensitive to a "physical change of the sample" to all orders. In this regard, it is worth noting that present-day precision spectroscopy can require long-term stability of spectral features at the 12th significant figure and higher [17,18]. Consequently, though one may seek to understand the general occurrence of isoclinic points in (for example) alkali-metal systems, an equally important question relates to how well the *ideal* isoclinic point can be realized in such systems. For example, in real systems alkali-metal isotopes often coexist, and even in a vapor of "pure" ^{87}Rb there is always some fractional component of ^{85}Rb with absorption lines that overlap (albeit slightly) those of ^{87}Rb as illustrated in Fig. 1. This overlap implies that Eq. (1) must be augmented with a third absorption cross section, complicating the simple argument leading to Eq. (5). Given the importance of ^{87}Rb in UAP, one must therefore question the extent to which ^{85}Rb "contamination" gives the isoclinic point a non-negligible temperature sensitivity. Moreover, since single-mode lasers are dominated by white frequency fluctuations, producing Lorentzian laser spectra with corresponding long tails [19], there will be an interaction between ^{85}Rb contamination and laser linewidth. Finally, for linearly polarized light an alignment among the ground-state Zeeman sublevels produced by optical pumping [20] could destroy the equality between the A and B cross sections, thereby giving the isoclinic point an alternate path to temperature sensitivity. Therefore, though isoclinic points may exist in the abstract, one is faced with the practical question of whether it is possible to realize spectroscopically useful isoclinic points in real alkali-metal systems.

III. THEORETICAL CONSIDERATIONS OF THE ALKALI-METAL D_1 ISOCLINIC POINT

As discussed more fully in Appendix A, the peak cross section for a D_1 transition in the alkali metals (i.e., $J_e = J_g = \frac{1}{2}$) originating from the $F_g = I + \frac{1}{2}$ ground-state hyperfine manifold is given by

$$\sigma_p(F_g F_e) = \sigma_o[J_g]\left[1 + \frac{2\langle \vec{I}\cdot\vec{S}\rangle}{(I+1)}\right] \times \begin{cases} \dfrac{(2I+3)(I+1)}{6(2I+1)^2} & F_e = I + \frac{1}{2} \\ \dfrac{2I(I+1)}{3(2I+1)^2} & F_e = I - \frac{1}{2} \end{cases}, \quad (6)$$

where $\langle \vec{I}\cdot\vec{S}\rangle$ is a measure of ground-state hyperfine polarization (i.e., the population imbalance between the two ground-state hyperfine levels) and σ_o is the integrated D_1 absorption cross section. (In our expressions we use the notation $[J] \equiv (2J+1)$.) Employing Whiting's second approximation [21] for a Voigt profile we can obtain a functional relationship between σ_o and the transition's oscillator strength, f:

$$\sigma_o = \frac{2\pi^2 r_o f c}{w_V\left[1.065 + 0.447\left(\frac{w_L}{w_V}\right) + 0.058\left(\frac{w_L}{w_V}\right)^2\right]}, \quad (7)$$

where r_o is the classical electron radius and w_L, w_D, and w_V correspond to the FWHM of the Lorentzian, Doppler, and Voigt profiles, respectively:

$$w_V = \frac{w_L}{2} + \sqrt{\frac{w_L^2}{4} + w_D^2}. \quad (8)$$

Similarly, for the D_1 transition originating from the $F_g = I - \frac{1}{2}$ hyperfine manifold,

$$\sigma_p(F_g F_e) = \sigma_o[J_g]\left[1 - \frac{2\langle \vec{I}\cdot\vec{S}\rangle}{I}\right] \times \begin{cases} \dfrac{2I(I+1)}{3(2I+1)^2} & F_e = I + \frac{1}{2} \\ \dfrac{I(2I-1)}{6(2I+1)^2} & F_e = I - \frac{1}{2} \end{cases}. \quad (9)$$

Then, writing Whiting's second approximation for the Voigt profile in detail, we have for the frequency dependence of the absorption cross sections

$$\sigma_{F_g F_e}\left(\Delta_{F_g F_e}\right) = \sigma_p(F_g F_e) G\left(\Delta_{F_g F_e}\right), \quad (10a)$$

where

$$G(\Delta_J) = \left[1 - \frac{w_L}{w_V}\right] e^{-4\ln(2)(\Delta_J/w_V)^2} + \left[\frac{w_L}{w_V}\right] \times \left[\frac{1}{1 + 4(\Delta_J/w_V)^2}\right] + \frac{1}{62.5}\left[1 - \frac{w_L}{w_V}\right]\left[\frac{w_L}{w_V}\right] \times \left\{e^{-0.4(|\Delta_J|/w_V)^{9/4}} - \frac{10}{10 + (|\Delta_J|/w_V)^{9/4}}\right\}, \quad (10b)$$

and the index J corresponds to one of the $F_g \rightarrow F_e$ resonances illustrated in Fig. 1.

Considering Eq. (6), it is clear that the two cross sections originating from the $F_g = I + \frac{1}{2}$ ground-state hyperfine manifold will be equal when $I = 3/2$, corresponding to the stable alkali-metal isotopes ^{7}Li, ^{23}Na, ^{39}K, ^{41}K, and ^{87}Rb. Thus, Eq. (5) predicts that there will be an isoclinic point midway between these two transitions. Of the alkali-metal isotopes with $I = 3/2$ shown in Table I, ^{87}Rb produces the largest vapor densities at the lowest temperatures, which has implications for UAP. Conversely, the two peak cross sections originating from the $F_g = I - \frac{1}{2}$ ground-state hyperfine manifold [i.e., Eq. (9)] are equal only for the unphysical case of $I = -5/2$. Thus, for the D_1 transition of the alkali-metal, excitation from $F_g = I - \frac{1}{2}$ *will not* yield an isoclinic point at an extremum of the absorption cross section.

An important point to note regarding Eq. (6) is that it was derived under the assumption that all Zeeman sublevels within a hyperfine manifold are equally populated (e.g., there is no polarization or alignment in the optically absorbing, ground-state hyperfine level). Consequently, under such conditions (which will be discussed further below) the absorption cross section will be *independent* of laser polarization, since no laser polarization parameters appear in Eq. (6). The corollary to this statement, which has relevance for precision spectroscopy, is that laser polarization can only have an effect on optical absorption to the extent that the population distribution among the

TABLE I. D_1 transition properties of various alkali-metal isotopes that would show an isoclinic point at an extremum of the $n^2S_{1/2}(F_g = 2) \rightarrow n^2P_{1/2}(F_e = 1,2)$ transitions. The temperatures were chosen to produce a vapor density of 10^{10} cm^{-3} for a vapor in equilibrium with its condensed phase; laser cooling and trapping could produce large vapor densities at lower temperatures and hence Doppler widths. Note that only in the case of ^{87}Rb will the two D_1 excited-state transitions be resolved relative to the Doppler width, which is given in the last column.

			$\Delta\nu_{hfs}$ (MHz)			
Alkali metal	Abundance (%)	1st resonance λ D_1 (nm)	$n^2S_{1/2}$	$n^2P_{1/2}$	T (°C)	$\Delta\nu_D$ (MHz)
^{7}Li	93%	670.8	803.5	92	291	2872
^{23}Na	100%	589.6	1771.6	189	114	1494
^{39}K	93%	769.9	461.7	58	53	806
^{41}K	7%	769.9	254.0	–	53	786
^{87}Rb	28%	794.8	6834.7	812	25	500

absorbing Zeeman sublevels is not uniform (e.g., that optical pumping creates a nonthermal population distribution among the Zeeman sublevels of a particular hyperfine manifold). An additional point to note is that since $\langle \vec{I} \cdot \vec{S} \rangle$ does not depend on F_e, any *hyperfine* polarization in the ground state will have no effect on the relative amplitude of the $F_g \rightarrow F_e = I \pm \frac{1}{2}$ optical transitions. Therefore, the degree of hyperfine polarization in the vapor will have no effect on the *frequency* of an alkali-metal D_1 isoclinic point, though it may affect the signal-to-noise ratio at an alkali-metal D_1 isoclinic point.

A. The ^{87}Rb D_1 isoclinic point and ^{85}Rb contamination

Though it is possible to procure isotopically enriched samples of ^{87}Rb, there will always be some level of ^{85}Rb "contamination" in the vapor. Unfortunately, as shown in Fig. 1 the wing of one of the ^{85}Rb resonances overlaps the $F_g = 2 \rightarrow F_e = 2$ transition of ^{87}Rb, destroying the exact equality between the two ^{87}Rb cross sections. An important question therefore concerns the extent to which this neighboring ^{85}Rb resonance destroys the isoclinic nature of the midpoint for realistic values of the ^{85}Rb isotope ratio.

Using the above equations, it is possible to calculate the frequency of the local minimum midway between the $5\,^2S_{1/2}(F_g = 2) \rightarrow 5\,^2P_{1/2}(F_e = 1,2)$ absorption lines of ^{87}Rb (transitions A and B in Fig. 1) as a function of the relative ^{85}Rb concentration. Briefly, we compute the cross section for each resonance and each isotope separately at a given laser frequency using Eq. (10a). We then sum the cross sections to evaluate the Beer's law attenuation of the laser and finally numerically determine the frequency near the midpoint where the derivative of the transmitted laser intensity is zero. The extent to which the frequency of this local minimum is insensitive to vapor temperature is a measure of how well the spectral feature approximates an ideal isoclinic point.

Defining η as the fractional abundance of ^{85}Rb in the vapor: $\eta \equiv N(^{85}\text{Rb})/[N(^{85}\text{Rb}) + N(^{87}\text{Rb})]$, the fractional frequency change per degree Celsius of the midpoint minimum, $\delta y/\delta T$, is shown in Fig. 2 as a function of vapor temperature for $\eta =$ 0.01, 0.03, and 0.1. For comparative purposes, we have also computed $\delta y/\delta T$ for the local maximum corresponding to the peak of the $5\,^2S_{1/2}(F_g = 1) \rightarrow 5\,^2P_{1/2}(F_e = 2)$ absorption line (i.e., transition D in Fig. 1). Of all the transitions in the ^{87}Rb D_1 spectrum, this is the most isolated, and therefore the resonance that comes closest to the ideal of a single resonance between two quantum states. Note that even for a ^{85}Rb abundance of 10%, the temperature sensitivity of the local minimum near the A-B transition midpoint is two orders of magnitude smaller than that of the peak frequency associated with transition D. Consequently, the isotope ratio in realizable samples of "pure" ^{87}Rb would appear to have little effect on the isoclinic nature of the midpoint minimum.

Figure 3 shows the influence of laser linewidth on $\delta y/\delta T$ for the A-B midpoint minimum. Laser linewidth is important, because the slowly falling Lorentzian wings of the line shape give the ^{87}Rb resonance an increased overlap with the ^{85}Rb absorption line (relative to the Gaussian wings of Doppler broadening). Note, however, that even for linewidths of 100 MHz, corresponding to VCSEL lasers at moderate injection currents above threshold [22], the A-B midpoint minimum acts very much like an ideal isoclinic point: $\delta y/\delta T < 10^{-12}$/°C. Moreover, $\delta y/\delta T$ for this midpoint is significantly less than the temperature sensitivity of the D transition's peak frequency for all laser linewidths.

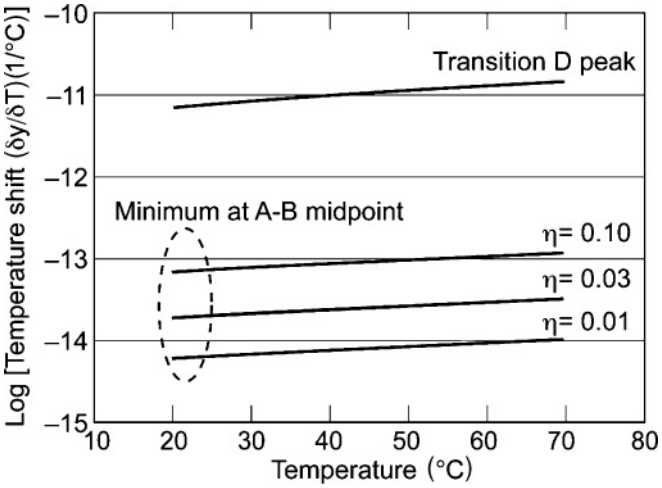

FIG. 2. Theoretical temperature shift of the minimum near the midpoint of the ^{87}Rb A and B transitions of Fig. 1 for differing values of the fractional abundance of ^{85}Rb in the vapor, η. Results are given in terms of fractional frequency, y (i.e., $y \equiv \delta\omega/\omega_o$). For comparison, the top curve shows the temperature shift of the peak frequency associated with transition D of Fig. 1, which is the most isolated transition in the spectrum. For these calculations, we chose a laser linewidth, Γ_F, of 100 kHz and a vapor length of 2.54 cm.

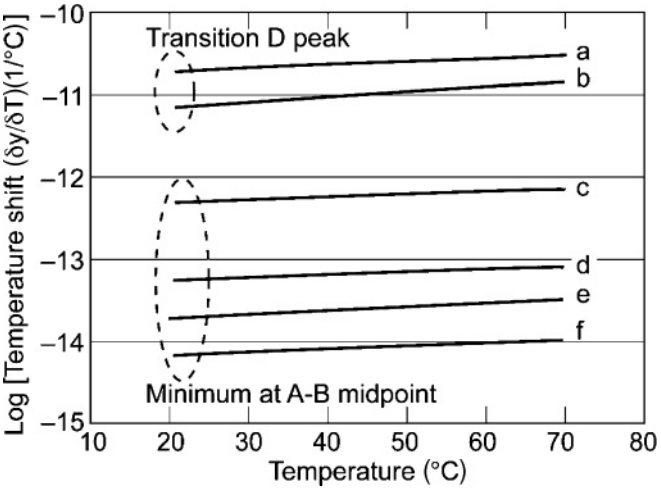

FIG. 3. Theoretical temperature shift of the minimum near the midpoint of the ^{87}Rb A and B transitions of Fig. 1 for differing values of the laser linewidth, Γ_F: (a) $\Gamma_F = 100$ MHz, (b) $\Gamma_F = 0.1$ MHz, (c) $\Gamma_F = 100$ MHz, (d) $\Gamma_F = 10$ MHz, (e) $\Gamma_F = 1$ MHz, and (f) $\Gamma_F = 0.1$ MHz. Results are given in terms of fractional frequency, y (i.e., $y \equiv \delta\omega/\omega_o$). For comparison, the top two curves show the temperature shift of the peak frequency associated with transition D of Fig. 1. For these calculations, we chose a 3% fractional abundance of ^{85}Rb, η, and a vapor length of 2.54 cm.

B. The ^{87}Rb D_1 isoclinic point and laser-generated ground-state alignment

Another mechanism that could potentially create an asymmetry in the two $5^2S_{1/2}$ $(F_g = 2) \rightarrow 5^2P_{1/2}$ $(F_e = 1,2)$ absorption lines is optical pumping. Though generation of a population imbalance between the two ground-state hyperfine manifolds (i.e., hyperfine polarization) will not produce an asymmetry as noted above, transfer of angular momentum from the photons of the light field to the ensemble of atoms could create a nonthermal population distribution among the $|F_g = 2\rangle$ Zeeman sublevels. Nonthermal population distributions couple differently to $|F_e = 1\rangle$ and $|F_e = 2\rangle$ and thereby can give rise to an asymmetry in the overlapped absorption doublet.

For linearly polarized light, as discussed more fully in Appendix B, the generation of a nonthermal population distribution among the ground-state Zeeman sublevels is dependent on a quadrupole moment of the excitation rate: $R_2(F_eF_g)$. The expression for this rate is derived in Appendix B and given by

$$R_2(F_eF_g) = \frac{3(-)^{F_g-F_e}}{2\sqrt{6}}[3\cos(2\theta)+1]\Phi_o\sigma_p(F_eF_g) \times G(\Delta_{F_eF_g})\sqrt{2F_g+1}\begin{Bmatrix} 1 & 1 & 2 \\ F_g & F_g & F_e \end{Bmatrix}, \quad (11)$$

where Φ_o is the photon flux, $\sigma_p(F_eF_g)$ and $G(\Delta_{F_eF_g})$ are given by Eqs. (6) and (10b), respectively, and θ is the angle between the atoms' quantization axis (along $\hat{z}$) and the laser's polarization direction in the $\hat{x}\hat{z}$ plane. For $\theta = \pi/2$, which corresponds to the most typical spectroscopic situation, Fig. 4(a) shows a normalized value of $R_2(F_eF_g)$ near the A-B midpoint minimum. In the figure we have normalized R_2 to the peak photon absorption rate for transition A in the absence of optical pumping: $\Phi_o\sigma_p(F_eF_g)$. Note that R_2 changes sign between the two excited-state hyperfine manifolds, indicative of the fact that excitation to one hyperfine level produces a positive alignment (via depopulation optical pumping) while excitation to the other creates a negative alignment. Figure 4(b) shows the magnitude of the normalized quadrupole excitation rate as a function of laser detuning on an expanded scale. As is readily apparent, when the laser is tuned within 10 MHz of the A-B midpoint minimum R_2 is reduced by more than two orders of magnitude relative to the nominal photon absorption rate. Consequently, without too drastic a reduction in light intensity, it should be possible to effectively eliminate optical pumping as a perturbation on the frequency of the midpoint minimum, again ensuring that it acts very much like an ideal isoclinic point.

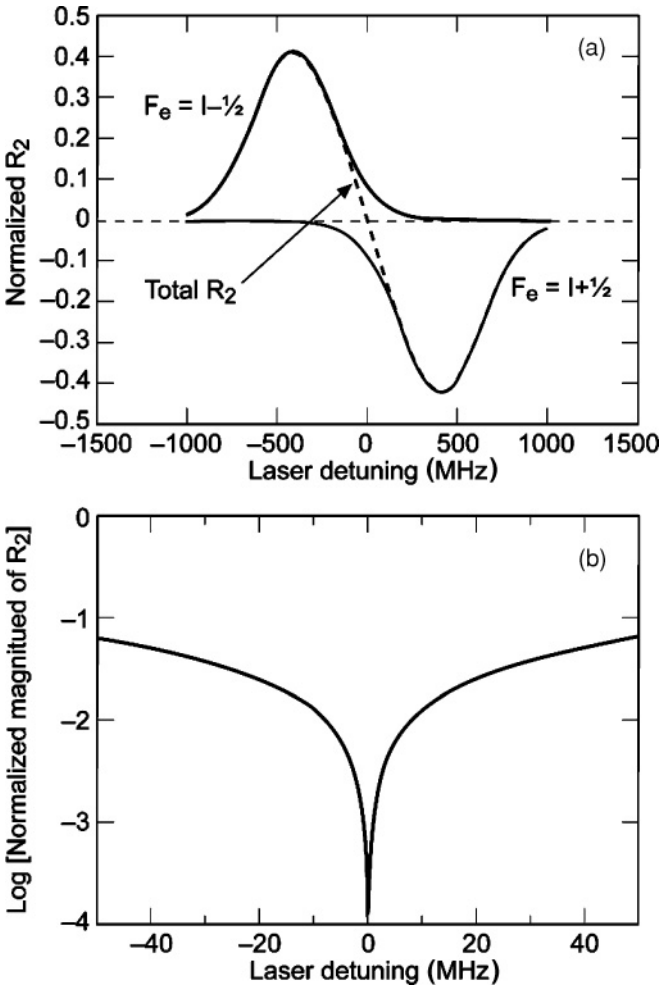

FIG. 4. (a) The quadrupole moment of the laser excitation rate, R_2, for an angle of $\pi/2$ between the atoms' quantization axis and the laser's (linear) polarization direction. Additionally, we assumed a temperature $T = 30$°C and a laser linewidth $\Gamma_F = 50$ MHz. R_2 is responsible for creating a nonthermal population distribution among the ground-state Zeeman sublevels of $|F_g\rangle$, and in this figure we have normalized R_2 to the peak photon absorption rate for transition A of Fig. 1. (b) The normalized magnitude of R_2 near the D_1 isoclinic point.

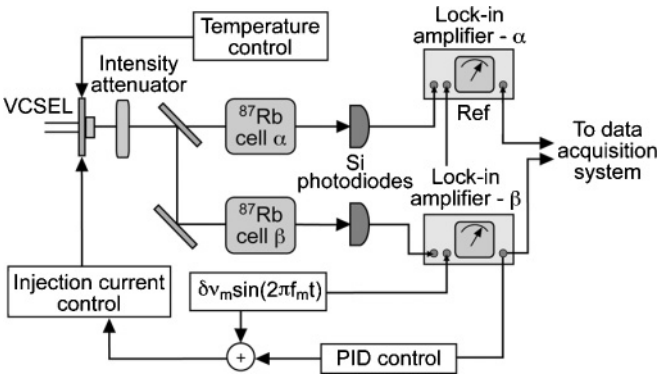

FIG. 5. Block diagram of the experimental arrangement. The injection current (and hence the laser frequency) was modulated at 40 kHz. The amplitude of this injection-current modulation corresponded to an optical-frequency modulation amplitude of 106 MHz. The intensity of the laser could be adjusted using a crossed polarizer.

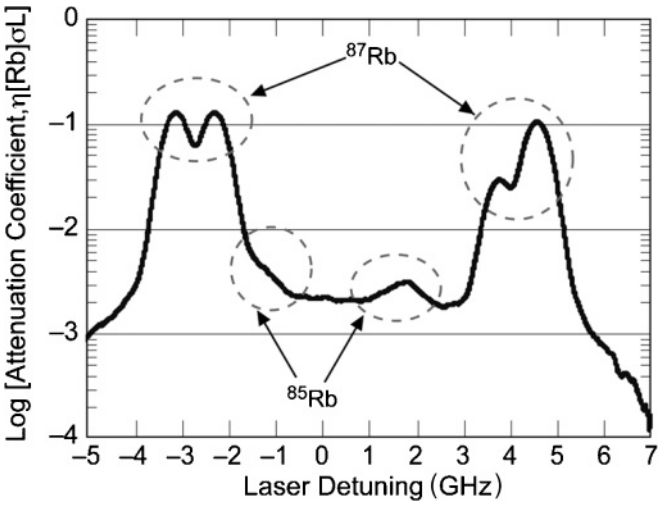

FIG. 6. Absorption spectrum of Rb in resonance cell β for a laser power of 15 μW; similar spectra were observed for various laser powers and also for resonance cell α. From the amplitude of the ^{85}Rb $F_g = 2 \rightarrow F_e = 2,3$ transition's well-isolated peak around +1.6 GHz, and the ^{87}Rb $F_g = 1 \rightarrow F_e = 2$ transition's peak around +4.4 GHz, we were able to estimate the ^{85}Rb isotope ratio in our absorption cells.

IV. EXPERIMENTAL DEMONSTRATION OF THE ALKALI-METAL D_1 ISOCLINIC POINT

Figure 5 shows a block diagram of our experimental arrangement. A VCSEL diode laser with a nominal output power of 300 μW had its wavelength modulated at 40 kHz and was then split into two beams. Each beam was attenuated with neutral density filters to 10 μW, and passed through two identical, cylindrical, Pyrex absorption cells. The beam diameter was approximately 0.5 cm. The commercially obtained absorption cells (i.e., Opthos Instruments, Inc.) contained isotopically enriched ^{87}Rb and had cell diameters of 2.54 cm and cell lengths equal to 2.54 cm. The light intensity transmitted through each resonance cell was detected with identical Si photodiodes and sent to two identical lock-in amplifiers (LIAs). Figure 6 shows an optical absorption spectrum for one of our cells at room temperature (i.e., [Rb] $= 2.1 \times 10^{10}$ cm^3 [23]), and from spectra like this we were able to determine that $\eta = (0.008 \pm 0.001)$ for our cells.

The output of LIA-β was first passed to a PID controller (proportional gain-integrator-differentiator) and then added to the modulation voltage sent to the VCSEL's injection-current controller. The VCSEL wavelength was thereby locked to some LAS feature of the D_1 Rb absorption spectrum as manifested in absorption cell β. In one set of experiments we locked the laser to the isoclinic point, midway between transitions A and B in Fig. 1, and in another set of experiments we locked the laser to the peak of transition D.

Absorption cell α acted as our frequency discriminator. Since the laser excited the same transition in cells α and β (e.g., the isoclinic point), the output of LIA-α was proportional to the frequency difference of that transition as manifested in the two cells. Holding the temperature of absorption cell α constant and changing the temperature of absorption cell β, we could then use the output of LIA-α to upper-bound the temperature shift of any absorption feature in the D_1 Rb spectrum. We calibrated the output of LIA-α by tuning the laser frequency and measuring the output voltage of LIA-α under open-loop conditions.

Since the diode laser's injection current is modulated, we not only create an oscillating laser frequency (FM), we also produce amplitude modulation (AM) of the laser intensity [7]. We therefore needed to exercise care in our measurements, since the concomitant amplitude modulation will produce an offset between the frequency the laser actually locks to and the local extremum-of-interest in the absorption spectrum. Specifically, when the lock-in amplifier demodulates the atomic absorption signal it outputs a voltage that is proportional to the first derivative of the LAS atomic line shape, which derives from the frequency modulation of the laser; this signal is dependent on the laser frequency's detuning from the extremum. In addition, however, regardless of atomic absorption the lock-in's output will contain an "offset" signal that is largely independent of laser frequency (but that is proportional to the laser's AM). Since the demodulated signal is the correction voltage that we feed back to lock the laser, any offset in the demodulated signal will shift the "locking point" of the laser from the line-shape extremum.

To be more specific, near the extremum of an absorption feature we can approximate the output of LIA-β as a linear function of the laser frequency's offset from the extremum $(\omega_L - \omega_J)$: $V_{\mathrm{LIA}-\beta} = \kappa(\omega_L - \omega_J) + \delta_{\mathrm{AM}}$. The proportionality coefficient κ is the slope of the correction signal (which is related to the second derivative of the line shape and also the amount of absorbed light), while the offset due to the laser's concomitant amplitude variations is given by δ_{AM}. If the number density of atoms in the vapor increases, the signal amplitude will obviously grow, implying that the slope κ is a temperature-dependent quantity. Alternatively, we expect δ_{AM} to be independent of vapor temperature to first order, especially if the vapor is optically thin as it is in our experiments (see Fig. 6). Clearly, the laser will lock to a frequency that yields $V_{\mathrm{LIA}-\beta} = 0$, or $\omega_L = \omega_J - \delta_{\mathrm{AM}}/\kappa$. Consequently, regardless of any atomic temperature shift inherent in ω_J, the locked laser's frequency can suffer a systematic temperature shift that depends on the ratio of δ_{AM} to κ.

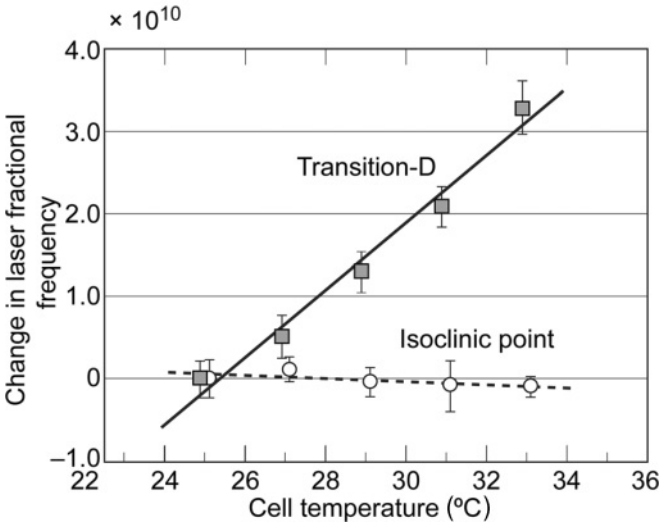

FIG. 7. Squares indicate the temperature shift of the peak frequency corresponding to transition D in Fig. 1 [i.e., $5\,^2S_{1/2}(F_g = 1) \rightarrow 5\,^2P_{1/2}(F_e = 2)$], while circles indicate the temperature shift of the D_1 isoclinic point. Not only is the temperature shift of the isoclinic point an order of magnitude smaller than that of transition D, but also to a 95% confidence level it cannot be distinguished from zero.

To eliminate this systematic temperature variation in our experiments, we removed resonance cell β from the laser beam path and zeroed the output of lock-in amplifier β. Essentially, we added a DC bias voltage to LIA-β that was equal and opposite to δ_{AM}. We then placed resonance cell β back into the beam path. Since the light-intensity loss by the cell's surfaces was minimal, and since δ_{AM} should be independent of laser frequency over the 7-GHz range of interest in our experiments, this procedure eliminated the "concomitant AM problem" to first order in our experiments. Though the concomitant AM problem may also be solved by third-harmonic locking, since the AM signal should have very little third-harmonic content, we found the simple bias-voltage subtraction method adequate for our purposes.

Figure 7 shows the principal results of the experimental work. We first locked the laser to the reasonably well-isolated ^{87}Rb D_1 transition shown in Fig. 1 (i.e., transition D). We then varied the temperature of cell β and determined the frequency change of this resonant feature by examining the output from LIA-α. The results showed a temperature shift of $(4.1 \pm 0.3) \times 10^{-11}/^{\circ}\mathrm{C}$ for transition D, which is consistent with the theoretical results shown in Fig. 3. (Note that the slight discrepancy between theory and experiment could be related to the limitations of Whiting's second approximation to the Voigt line shape.) We then locked the laser to the ^{87}Rb D_1 isoclinic point. Again, we varied the temperature of cell β and determined the isoclinic point's frequency change by examining the output of LIA-α. In the case of the isoclinic point, the results showed a temperature shift of $-(2.0 \pm 1.4) \times 10^{-12}/^{\circ}\mathrm{C}$. Not only was the isoclinic point's temperature shift an order of magnitude lower than transition D's, but at the 95% confidence level we could not distinguish a difference between the isoclinic point's temperature shift and zero.

V. SUMMARY

Ultraminiature atomic physics, as exemplified by chip-scale atomic clocks and chip-scale atomic magnetometers, is motivating the investigation of atomic physics under physical conditions not routinely encountered in the laboratory (e.g., high alkali-metal densities or atomic systems probed with stochastic fields) and also forcing a re-examination of problems that (to a large extent) have been considered "solved." An example of this latter situation concerns the problem of overlapped atomic absorption lines arising from Doppler broadening, where spectral features exhibit a temperature sensitivity due to the Doppler width's temperature dependence. Since the shift of an optical absorption line depends on the extent to which overlapping transitions pull its peak frequency, Doppler-broadened transitions routinely exhibit temperature-dependent shifts in their resonant frequencies. Though sub-Doppler spectroscopic techniques can mitigate the spectral pulling, such techniques are often at odds with the constraints of UAP: increasing the power-budget of UAP systems and creating potential sensitivities to microphonics.

In the present work, we have reconsidered the spectroscopic problem of obtaining stable resonant features in linear absorption spectroscopy (LAS), and in particular have introduced the concept of spectroscopic isoclinic points for this purpose (i.e., "[a] wavelength, wave number, or frequency at which the first derivative of an absorption spectrum of a sample does not change upon a chemical reaction or physical change of the sample" [14]). More specifically, we have demonstrated that isoclinic points can be found in the D_1 optical spectra of the alkali metals with $I = 3/2$, and we investigated the first resonance D_1 isoclinic point of ^{87}Rb in detail.

Even considering the contamination of isotopically enriched samples of ^{87}Rb ($I = 3/2$) with ^{85}Rb ($I = 5/2$) and the (potentially) long Lorentzian wings of laser line shapes, theory shows that the alkali-metal isoclinic point remains orders of magnitude less sensitive to temperature variations than any other resonant feature in the atoms' absorption spectrum. Additionally, theory shows that the creation of a ground-state alignment by optical pumping cannot take place with a laser tuned to the isoclinic point, so the isoclinic point's frequency should also be independent of laser intensity.

To demonstrate the existence of a D_1 isoclinic point in the alkali metals, we performed an experiment to measure the temperature shift of the extremum midway between the $5\,^2S_{1/2}(F_g = 2) \rightarrow 5\,^2P_{1/2}(F_e = 1,2)$ transitions of ^{87}Rb (i.e., the presumed D_1 isoclinic point) and compared this to the temperature shift of the $5\,^2S_{1/2}(F_g = 1) \rightarrow 5\,^2P_{1/2}(F_e = 2)$ transition. The latter atomic transition is the most isolated transition in the Rb atom's first resonance spectrum, and therefore the least sensitive to spectral overlap issues. Not only did we find that the isoclinic point had a temperature shift more than an order of magnitude smaller than that of the $5\,^2S_{1/2}(F_g = 1) \rightarrow 5\,^2P_{1/2}(F_e = 2)$ transition, but to a 95% confidence level we could not differentiate the isoclinic point's temperature shift from zero. These results support the theoretical claims for an isoclinic point in the D_1 optical spectra of $I = 3/2$ alkali metals and suggest the potential benefits of such isoclinic points in ultraminiature atomic physics.

ACKNOWLEDGMENTS

The authors thank B. Jaduszliwer for a number of stimulating discussions regarding this work and Dylan Caponi for help in performing several of the experiments. Additionally, the authors acknowledge the participation of A. Matsko, L. Maleki, A. Savchenkov, D. Seidel, V. Ilchenko, and M. Mohageg of OEwaves in the DARPA-funded project under which this work was supported (Contract No. AERO9012058).

APPENDIX A: D_1 ABSORPTION CROSS SECTIONS

In this appendix we focus attention on the four $F_g = I \pm \frac{1}{2} \rightarrow F_e = I \pm \frac{1}{2}$ transitions in the alkali-metal D_1 spectrum (i.e., $n^2S_{1/2} \rightarrow m^2P_{1/2}$), where I is the nuclear spin. Though we will mostly be interested in first resonance transitions (i.e., $m = n$), the analysis will be valid for other transitions (e.g., the second resonance transitions with $m = n + 1$). Our purpose is to derive the optical absorption cross section for an arbitrary $n^2S_{1/2}(F_g) \rightarrow m^2P_{1/2}(F_e)$ transition as a function of laser linewidth and ground-state hyperfine polarization. For notational convenience, we will follow Happer [4] and define the total angular-momentum quantities a and b as $a = I + \frac{1}{2}$ and $b = I - \frac{1}{2}$.

Since the optical absorption cross section is related to the expectation value of the induced dipole moment in the vapor (actually its squared magnitude), we write the peak absorption cross section for an $F_g \rightarrow F_e$ transition, $\sigma_p(F_gF_e)$, as

$$\sigma_p(F_gF_e) \sim \mathrm{Tr}[\rho(\hat{\xi}\cdot\vec{r})(\hat{\xi}\cdot\vec{r})^*], \tag{A1}$$

where $\mathrm{Tr}[\cdots]$ corresponds to the trace operation, ρ is the density matrix operator for the atomic system, and $\hat{\xi}$ corresponds to the unit vector describing the field's polarization state. Writing Eq. (A1) in full detail, we have

$$\sigma_p(F_gF_e) \sim \sum_{\substack{m_g,f,M,\\ f',M'}} \langle F_gm_g|\rho|fM\rangle\langle fM|(\hat{\xi}\cdot\vec{r})|f'M'\rangle \times \langle f'M'|(\hat{\xi}\cdot\vec{r})^*|F_gm_g\rangle. \tag{A2}$$

If we now assume that there is no atomic population in the excited state, and that there are no coherences between atomic eigenstates (both of which are valid approximations given the weak fields of interest in the present work), then

$$\langle F_gm_g|\rho|fM\rangle = \rho(F_gm_g)\delta_{F_g,f}\delta_{m_g,M}, \tag{A3}$$

where $\rho(F_gm_g)$ is simply the fractional atomic population in the $|F_gm_g\rangle$ eigenstate. Further, given the electric dipole nature of the second and third matrix elements in Eq. (A2), we must have $f' = F_e$ and $f = F_g$. With these constraints, Eq. (A2) becomes

$$\sigma_p(F_gF_e) \sim \sum_{m_g,m_e} \rho(F_gm_g)|\langle F_gm_g|(\hat{\xi}\cdot\vec{r})|F_em_e\rangle|^2. \tag{A4}$$

To proceed, we now consider an arbitrarily polarized light beam, so working in spherical coordinates

$$\hat{\xi}\cdot\vec{r} = \sum_{\mu}(-1)^{\mu}\xi_{-\mu}r_{\mu}, \tag{A5}$$

where ξ_μ corresponds to the degree of left-circularly polarized (ξ_{-1}), right-circularly polarized (ξ_1), or π-polarized (ξ_0) light in the field. Employing Eq. (A5) in Eq. (A4) then yields

$$\sigma_p(F_gF_e) \sim \sum_{\substack{m_g,m_e\\ \mu,\nu}} (-)^{\mu-\nu}\rho(F_gm_g)\xi_{-\mu}\xi_{\nu}\langle F_gm_g|r_{\mu}|F_em_e\rangle \times \langle F_em_e|r_{-\nu}|F_gm_g\rangle. \tag{A6}$$

Taking advantage of the Wigner-Eckart theorem to evaluate the matrix elements [24,25], and assuming that the atomic population is uniform among the Zeeman sublevels of a particular ground-state hyperfine manifold (e.g., that optical pumping does not lead to a ground-state polarization or alignment [26]), we have

$$\sigma_p(F_gF_e) \sim (-)^{F_g+F_e}|\langle F_g||r||F_e\rangle|^2\frac{\rho(F_g)}{[F_g]}\sum_{\mu\nu}(-)^{\mu}\xi_{-\mu}\xi_{\nu} \times \sum_{m_g,m_e}\begin{pmatrix}F_e & F_g & 1\\ m_e & -m_g & \mu\end{pmatrix}\begin{pmatrix}F_e & F_g & 1\\ m_e & -m_g & \nu\end{pmatrix}, \tag{A7}$$

where $\rho(F_g)$ is defined as $\sum_{m_g}\rho(F_g,m_g)$ and $[F_g] \equiv (2F_g + 1)$. Of course, from the orthogonality of the $3j$ symbols, the second sum in Eq. (A7) just equals $\delta_{\mu\nu}/3$, so that Eq. (A7) becomes

$$\sigma_p(F_gF_e) \sim (-)^{F_g+F_e}|\langle F_g||r||F_e\rangle|^2\frac{\rho(F_g)}{3[F_g]}\sum_{\nu}(-)^{\nu}\xi_{-\nu}\xi_{\nu}. \tag{A8}$$

By definition the sum over the laser polarization components ξ_ν is unity. Consequently, after writing the reduced matrix element in terms of the uncoupled angular momenta (i.e., J_g, J_e, and I), where J is the electronic angular momentum (spin plus orbital), we arrive at

$$\sigma_p(F_gF_e) \sim (-)^{J_e+J_g+2I}\frac{[F_e]\rho(F_g)}{3}\begin{Bmatrix}J_e & F_e & I\\ F_g & J_g & 1\end{Bmatrix}^2|\langle J_g||r||J_e\rangle|^2 \tag{A9}$$

or

$$\sigma_p(F_gF_e) \sim (-)^{J_e+J_g+2I}\frac{[F_e][F_g]}{6[I]}\left(1+\frac{8(F_g-I)}{[F_g]}\langle\vec{I}\cdot\vec{S}\rangle\right) \times \begin{Bmatrix}J_e & F_e & I\\ F_g & J_g & 1\end{Bmatrix}^2|\langle J_g||r||J_e\rangle|^2. \tag{A10}$$

Here, $\langle\vec{I}\cdot\vec{S}\rangle$ is a measure of ground-state hyperfine polarization: for $\langle\vec{I}\cdot\vec{S}\rangle$ equal to $+I/2$, the nuclear and electronic spin orientations are maximally aligned, while for $\langle\vec{I}\cdot\vec{S}\rangle$ equal to $-(I+1)/2$ the nuclear and electronic spin orientations are maximally antialigned.

Evaluating the $6j$ symbols for the case of interest: $J_e = J_g = \frac{1}{2}$, and $F_g = a = I + \frac{1}{2}$, we obtain

$$\sigma_p(F_g F_e) \sim \frac{|\langle J_g||r||J_e\rangle|^2}{3}\left(1 + \frac{2\langle \vec{I}\cdot\vec{S}\rangle}{(I+1)}\right) \times \begin{cases} \dfrac{(2I+3)(I+1)}{6(2I+1)^2} & F_e = a \\ \dfrac{2I(I+1)}{3(2I+1)^2} & F_e = b \end{cases}, \quad \text{(A11)}$$

and performing the same analysis for $F_g = b = I - \frac{1}{2}$, we obtain

$$\sigma_p(F_g F_e) \sim \frac{|\langle J_g||r||J_e\rangle|^2}{3}\left(1 - \frac{2\langle \vec{I}\cdot\vec{S}\rangle}{I}\right) \times \begin{cases} \dfrac{2I(I+1)}{3(2I+1)^2} & F_e = a \\ \dfrac{I(2I-1)}{6(2I+1)^2} & F_e = b \end{cases}. \quad \text{(A12)}$$

Note that these expressions are valid for any of the D_1 transitions of an alkali-metal atom. For example, in the case of Rb these expressions are valid for the first resonance transition at 794.8 nm as well as the second resonance transition at 421.5 nm. The differences among the various $n \to m$ transitions reside in the reduced matrix elements of Eqs. (A11) and (A12).

To proceed, we express the reduced matrix element in terms of the D_1 transition's oscillator strength. To this end, we first sum Eq. (A10) over F_e and F_g in the case that $\langle \vec{I}\cdot\vec{S}\rangle$ is zero, obtaining

$$\sum_{F_g,F_e}\sigma_p(F_g F_e) \equiv \sigma_o = K\frac{|\langle J_g||r||J_e\rangle|^2}{6[I][J_g]} \times \sum_{F_g}[F_g]\sum_{F_e}[F_e][J_g]\begin{Bmatrix} J_e & F_e & I \\ F_g & J_g & 1\end{Bmatrix}^2, \quad \text{(A13a)}$$

or

$$\sigma_o = K\frac{|\langle J_g||r||J_e\rangle|^2}{3[J_g]}, \quad \text{(A13b)}$$

where K is a proportionality constant. Identifying σ_o with the peak absorption cross section of a Voigt profile for *unresolved* hyperfine structure, we can take advantage of the area theorem for an absorption line [27]:

$$\int_0^\infty \sigma(\omega_L)\,d\omega_L = 2\pi^2 r_o f c. \quad \text{(A14)}$$

Here, r_o is the classical electron radius, f is the oscillator strength of the transition, and c is the speed of light. (For the first resonance D_1 transition of Rb at 794.8 nm $f = 0.33$, while $f = 0.0037$ for the second resonance D_1 transition at 421.5 nm [28].) Then, employing Whiting's second approximation [21] for a Voigt line shape, we relate the peak cross section, σ_o, to the total cross section:

$$\sigma_o = \frac{2\pi^2 r_o f c}{w_V\left[1.065 + 0.447\left(\frac{w_L}{w_V}\right) + 0.058\left(\frac{w_L}{w_V}\right)^2\right]}, \quad \text{(A15)}$$

which allows us to relate the reduced matrix element to the oscillator strength. In Eq. (A15), w_L, w_D, and w_V equal the FWHM of the Lorentzian profile, the Doppler profile, and the Voigt profile, respectively:

$$w_V = \frac{w_L}{2} + \sqrt{\frac{w_L^2}{4} + w_D^2}, \quad \text{(A16a)}$$

$$w_D = 2\omega_o\sqrt{\frac{2kT\ln(2)}{Mc^2}}, \quad \text{(A16b)}$$

and

$$w_L = A + \Gamma_F. \quad \text{(A16c)}$$

In these expressions, A is the Einstein A coefficient of the transition [29] and Γ_F is the FWHM of the laser field. To include laser linewidth into the theory, we have simply added its width to the atom's natural dephasing rate, which is valid for a single-mode field suffering phase diffusion [30–32].

APPENDIX B: QUADRUPOLE MOMENT OF THE OPTICAL EXCITATION RATE

In this appendix, we want to consider the generation of multipole moments in the ground-state density matrix due to depopulation optical-pumping [4] of a given ground-state hyperfine level, F_g. In particular, we want to consider the generation of ground-state alignment in F_g when a linearly polarized laser is tuned to the D_1 isoclinic point. To begin, we write the optical excitation rate out of a particular eigenstate $|F_g,m_g\rangle$ as

$$R_{F_e F_g}(m_g) = \sum_{m_e} R_{F_e F_g}(m_e,m_g) = \Phi(\omega_L)\sum_{m_e}|\langle F_g m_g|\hat{\xi}\cdot\vec{r}|F_e m_e\rangle|^2, \quad \text{(B1)}$$

where Φ is proportional to the light irradiance and is also dependent on the laser frequency ω_L through the laser's detuning from an atomic resonance frequency, $\hat{\xi}$ is the normalized polarization vector of the laser, and $\vec{r}$ is the dipole-moment operator for the atom. Note that from Eq. (A4), $R_{F_e F_g}(m_g)$ is related to the optical absorption cross section:

$$\sigma_p(F_g F_e) \sim \frac{1}{\Phi(\omega_L)}\sum_{m_g}\rho(F_g m_g)R_{F_e F_g}(m_g), \quad \text{(B2)}$$

so from Eq. (A7) we have

$$R_{F_e F_g}(\mathrm{m_g}) = (-)^{F_g+F_e}\Phi(\omega_L)|\langle F_g||r||F_e\rangle|^2 \times \sum_{m_e\mu}(-)^\mu \xi_{-\mu}\xi_\mu\begin{pmatrix} F_e & F_g & 1 \\ m_e & -m_g & \mu\end{pmatrix}^2. \quad \text{(B3)}$$

We now expand the excitation rate in terms of a spherical basis set of functions. Specifically, we write

$$R_{F_eF_g}(m_g) = \sum_{KQ} R_{KQ}(F_eF_g) g_{KQ}(F_g m_g), \tag{B4}$$

where the g_{KQ} are spherical basis functions [4] and the R_{KQ} describe the decomposition of our excitation rate in terms of these spherical basis components. Since we do not generate coherences among the ground-state Zeeman sublevels of F_g, only the $Q = 0$ terms are nonzero. Thus, writing the g_{KQ} in terms of $3j$ symbols dropping the superfluous Q descriptor we have

$$g_K(F_g m_g) = (-1)^{F_g - m_g}\sqrt{2K+1}\begin{pmatrix} F_g & F_g & K \\ m_g & -m_g & 0 \end{pmatrix}. \tag{B5}$$

Taking advantage of the orthonormality of the g_K, we then get

$$\begin{aligned} &R_K(F_eF_g) \\ &= \Phi(\omega_L)\sqrt{2K+1}|\langle F_g||r||F_e\rangle|^2 \sum_{m_g,m_e,\mu} (-)^{F_e-m_e}\xi_{-\mu}\xi_{\mu} \\ &\quad\times \begin{pmatrix} F_g & F_g & K \\ -m_g & m_g & 0 \end{pmatrix}\begin{pmatrix} F_g & 1 & F_e \\ m_g & \mu & -m_e \end{pmatrix}^2. \end{aligned} \tag{B6}$$

To proceed further, we consider linear polarized light, with the propagation direction of our laser beam, $\hat{y}$, *perpendicular* to the atom's quantization axis, $\hat{z}$; this allows us to consider $m_g - m_e = \pm 1$ optical transitions as well as $m_g - m_e = 0$ transitions in a single expression. (Note that propagation of the laser in a direction *parallel* to the quantization axis is equivalent to what we consider here when the laser's polarization is perpendicular to $\hat{z}$: $m_g - m_e = \pm 1$ transitions.) Consequently, we write $\xi_{-1}\xi_1$ and $\xi_0\xi_0$ in terms of the angle between the atom's quantization axis and the laser's polarization direction, θ:

$$\xi_{-1}\xi_1 = \xi_1\xi_{-1} = -\tfrac{1}{2}\sin^2(\theta), \tag{B7a}$$

$$\xi_0\xi_0 = c\cos^2(\theta). \tag{B7b}$$

The sum over μ in Eq. (B6) now becomes

$$\begin{aligned} &\sum_{\mu}\xi_{-\mu}\xi_{\mu}\begin{pmatrix} F_g & 1 & F_e \\ m_g & \mu & -m_e \end{pmatrix}^2 \\ &= -\frac{\sin^2(\theta)}{2}\sum_{\mu}\begin{pmatrix} F_g & 1 & F_e \\ m_g & \mu & -m_e \end{pmatrix}^2 \\ &\quad + \left(\cos^2(\theta) + \frac{\sin^2(\theta)}{2}\right)\begin{pmatrix} F_g & 1 & F_e \\ m_g & 0 & -m_e \end{pmatrix}^2. \end{aligned} \tag{B8}$$

Then, employing Eq. (B8) in Eq. (B6) and taking advantage of the $3j$ symbol contraction yields, after a bit of algebra,

$$R_0(F_eF_g) = \frac{\Phi(\omega_L)|\langle F_g||r||F_e\rangle|^2}{3\sqrt{2F_g+1}}, \tag{B9a}$$

$$R_1(F_eF_g) = 0, \tag{B9b}$$

and

$$\begin{aligned} R_2(F_eF_g) &= \frac{(-)^{F_g-F_e}\Phi(\omega_L)}{2\sqrt{6}}(3\cos(2\theta)+1) \\ &\quad\times \begin{Bmatrix} 1 & 1 & 2 \\ F_g & F_g & F_e \end{Bmatrix}|\langle F_g||r||F_e\rangle|^2, \end{aligned} \tag{B9c}$$

with all $R_K(F_e, F_g) = 0$ for $K \geqslant 3$ due to the fact that we are dealing with single-photon dipole transitions. Finally, we write the reduced matrix element in terms of the electronic angular momentum J and allow $\Phi(\omega_L) \to \Phi(\omega_L)|\langle J_g \parallel r \parallel J_e\rangle|^2$:

$$R_0(F_eF_g) = \frac{\Phi(\omega_L)}{3}[F_e]\sqrt{2F_g+1}\begin{Bmatrix} J_g & F_g & I \\ F_e & J_e & 1 \end{Bmatrix}^2, \tag{B10a}$$

$$\begin{aligned} R_2(F_eF_g) &= \frac{(-)^{F_g-F_e}\Phi(\omega_L)}{2\sqrt{6}}(3\cos(2\theta)+1)[F_e][F_g] \\ &\quad\times \begin{Bmatrix} 1 & 1 & 2 \\ F_g & F_g & F_e \end{Bmatrix}\begin{Bmatrix} J_g & F_g & I \\ F_e & J_e & 1 \end{Bmatrix}^2. \end{aligned} \tag{B10b}$$

Noting that $R_0(FeFg)$ must be given by $\Phi_o\,\sigma_{FeFg}(\Delta_{FeFg})$, where Φ_o is the photon flux and $\sigma_{FeFg}(\Delta_{FeFg})$ is the absorption cross section given by Eq. (10a), the expressions for R_0 and R_2 can be further simplified:

$$R_0(F_eF_g) = \Phi_o\sigma_p(F_eF_g)G\left(\Delta_{F_eF_g}\right), \tag{B11a}$$

$$\begin{aligned} R_2(F_eF_g) &= \frac{3(-)^{F_g-F_e}}{2\sqrt{6}}(3\cos(2\theta)+1)\Phi_o\sigma_p(F_eF_g) \\ &\quad\times G\left(\Delta_{F_eF_g}\right)\sqrt{2F_g+1}\begin{Bmatrix} 1 & 1 & 2 \\ F_g & F_g & F_e \end{Bmatrix}. \end{aligned} \tag{B11b}$$

Considering Eqs. (B11), it is clear that the laser's polarization contributes only to the quadrupole moment of the excitation rate, R_2; and so it is only through this term that angular momentum can be transferred from the light field to the atoms, thereby creating a nonthermal population distribution among the ground-state Zeeman sublevels.

[1] S. Knappe, V. Shah, P. D. D. Schwindt, L. Hollberg, J. Kitching, L.-A. Liew, and J. Moreland, Appl. Phys. Lett. **85**, 1460 (2004).

[2] R. Lutwak, J. Deng, W. Riley, M. Varghese, J. Leblanc, G. Tepolt, M. Mescher, D. K. Serkland, K. M. Geib, and G. M. Peake, in *Proc. 36th Annual Precise Time and Time Interval (PTTI) Systems and Applications Meeting* (US Naval Observatory, Washington DC, 2004), pp. 339–354.

[3] P. D. D. Schwindt, S. Knappe, V. Shah, L. Hollberg, J. Kitching, L.-A. Liew, and J. Moreland, Appl. Phys. Lett. **85**, 6409 (2004).

[4] W. Happer, Rev. Mod. Phys. **44**, 169 (1972).

[5] N. D. Bhaskar, J. Camparo, W. Happer, and A. Sharma, Phys. Rev. A **23**, 3048 (1981).

[6] I. M. Savukov and M. V. Romalis, Phys. Rev. A **71**, 023405 (2005).

[7] J. C. Camparo, Contemp. Phys. **26**, 443 (1985).

[8] H. Furuta and M. Ohtsu, Appl. Opt. **28**, 3737 (1989).

[9] M. Têtu, N. Cyr, B. Villeneuve, S. Thériault, M. Breton, and P. Tremblay, IEEE Trans. Instrum. Meas. **40**, 191 (1991).

[10] B. S. Mathur, H. Tang, and W. Happer, Phys. Rev. **171**, 11 (1968).
[11] B. R. Bulos, A. Marshall, and W. Happer, Phys. Rev. A **4**, 51 (1971).
[12] A. L. Schawlow, Rev. Mod. Phys. **54**, 697 (1982).
[13] See, for example, D. C. Heinecke, A. Bartels, T. M. Fortier, D. A. Braje, L. Hollberg, and S. A. Diddams, Phys. Rev. A **80**, 053806 (2009).
[14] IUPAC, *Compendium of Chemical Terminology*, 2nd ed., compiled by A. D. McNaught and A. Wilkinson (Blackwell Scientific, Oxford, 1997).
[15] T. B. Marriott and O. H. Griffith, J. Magn. Reson. **13**, 45 (1974).
[16] V. A. Barnett and D. D. Thomas, Biochem. **26**, 314 (1987).
[17] J. Ye, S. Swartz, P. Jungner, and J. L. Hall, Opt. Lett. **21**, 1280 (1996).
[18] J. Vanier and C. Mandache, Appl. Phys. B **87**, 565 (2007).
[19] P. Zoller and P. Lambropoulos, J. Phys. B: Atom. Molec. Phys. **12**, L547 (1979).
[20] M. Auzinsh, D. Budker, and S. M. Rochester, Phys. Rev. **80**, 053406 (2009).
[21] E. E. Whiting, J. Quant. Spectrosc. Radiat. Transfer **8**, 1379 (1968).
[22] M. B. Willemsen, A. S. van de Nes, M. P. van Exter, J. P. Woerdman, M. Kicherer, R. King, R. Jäger, and K. J. Ebeling, J. Appl. Phys. **89**, 4183 (2001).
[23] T. J. Killian, Phys. Rev. **27**, 578 (1926).
[24] M. E. Rose, *Elementary Theory of Angular Momentum* (Wiley, New York, 1957).
[25] K. Blum, *Density Matrix Theory and Applications* (Plenum, New York, 1981).
[26] Our constraint regarding a uniform population distribution among the Zeeman sublevels is not necessarily a limitation on the photon absorption rate (i.e., optical pumping rate). We are simply assuming that angular momentum is not transferred from the light field to the atomic vapor, which could be achieved with unpolarized light. A linear polarized laser field can be made to appear unpolarized to the atoms, if the laser's polarization vector is properly oriented relative to the atoms' quantization axis.
[27] A. C. G. Mitchell and M. W. Zemansky, *Resonance Radiation and Excited Atoms* (Cambridge, London, 1971), Chap. III.
[28] L. N. Shabanova and A. N. Khlyustalov, Opt. Spectrosc. (USSR) **56**, 128 (1984).
[29] U. Volz and H. Schmoranzer, Phys. Scr., T **65**, 48 (1996).
[30] J. H. Eberly, Phys. Rev. Lett. **37**, 1387 (1976).
[31] A. T. Georges and P. Lambropoulos, Phys. Rev. A **18**, 587 (1978).
[32] J. G. Coffer, M. Anderson, and J. C. Camparo, Phys. Rev. A **65**, 033807 (2002).